



# Theoretical modeling and design of some pyrazolopyrimidine derivatives as *Wolbachia* inhibitors, targeting lymphatic filariasis and onchocerciasis

Fabian Audu Ugbe<sup>1</sup> · Gideon Adamu Shallangwa<sup>1</sup> · Adamu Uzairu<sup>1</sup> · Ibrahim Abdulkadir<sup>1</sup>

Received: 2 January 2022 / Accepted: 10 April 2022

© The Author(s), under exclusive licence to Springer-Verlag GmbH Germany, part of Springer Nature 2022

## Abstract

Lymphatic filariasis and onchocerciasis are two common filarial diseases caused by a group of parasitic nematodes called filarial worms, which play host to the bacteria organism *Wolbachia*. One good treatment approach seeks *Wolbachia* as drug target. Here, a QSAR study was conducted to investigate the anti-*wolbachia* activities ( $pEC_{50}$ ) of 52 pyrazolopyrimidine analogues, while using the built model to predict the  $pEC_{50}$  values of the newly designed analogues. Density Functional Theory was used for the structural optimization, while the model building was based on Genetic Function Algorithm approach. The built QSAR model was validated thus:  $R^2=0.8104$ ,  $R^2_{adj}=0.7629$ ,  $Q^2_{cv}=0.6981$ ,  $R^2_{test}=0.7501$  and  $cRp^2=0.7476$ . The predicted  $pEC_{50}$  of all newly designed compounds were higher than that of the template (**43**). The new compounds were; observed to pass the drug-likeness criteria, uniformly distributed to the brain, and found to be non-mutagenic. Also, the new compounds and the reference drug (doxycycline), were docked onto Ovarian Tumor (OTU) deubiquitinase receptor (PDB ID: 6W90) using iGEMDOCK tool. This protein is known to help *Wolbachia* subvert host ubiquitin signaling. The resulting binding scores of the newly designed compounds except **A5** were higher than that of doxycycline, while the protein–ligand interactions were majorly characterized by Hydrogen-bonding and hydrophobic interaction types. Therefore, the newly designed molecules could be developed as potential drug candidates for the treatment of lymphatic filariasis and onchocerciasis.

**Keywords** Density functional theory · Filarial diseases · Molecular docking · Pharmacokinetics · QSAR · *Wolbachia*

## Abbreviations

AD	Applicability domain	DFT	Density functional theory
ADMET	Absorption, distribution, metabolism, excretion, and toxicity	DTC	Drug theoretical and cheminformatics
AIDS	Acquired immuno-deficiency syndrome	EC <sub>50</sub>	Half-maximal effective concentration
ALA	Alanine	$pEC_{50}$	Negative log of EC <sub>50</sub>
ARG	Arginine	ESOL	Estimated solubility
ASN	Asparagine	LOF	Friedman lack-of-fit
ASP	Aspartic acid	GFA	Genetic function approximation
BBB	Blood brain barrier	GLN	Glutamine
LogBB	Logarithmic ratio of brain to plasma drug concentration	GLU	Glutamic acid
B3LYP	Becke's three-parameter read-Yang-Parr hybrid	GLY	Glycine
		h*	Warning leverage
		HIA	Human intestinal absorption
		HIS	Histidine
		HIV	Human immuno-deficiency virus
		HBA	Hydrogen bond acceptor
		HBD	Hydrogen bond donor
		H-Bond	Hydrogen bond
		ILE	Isoleucine
		LEU	Leucine

✉ Fabian Audu Ugbe  
ugbefabianaudu@gmail.com

<sup>1</sup> Department of Chemistry, Faculty of Physical Sciences, Ahmadu Bello University, P.M.B. 1044, Zaria, Kaduna State, Nigeria

LYS	Lysine
MDA	Mass Drug Administration
MRTD	Maximum recommended tolerated dose
ME	Mean Effect
MLogP	Lipophilicity
MMFF	Molecular mechanics force field
MW	Molecular weight
MLR	Multi-linear regression
NTD	Neglected tropical diseases
OUT	Ovarian tumor
PaDEL	Pharmaceutical Data Exploration Laboratory
PDB	Protein Data Bank
PHE	Phenylalanine
PRO	Proline
LogPS	Blood–brain permeability-surface area product
QSAR	Quantitative structure activity relationship
RO5	Rule of five
SER	Serine
SEE	Standard error of estimation
THR	Threonine
TPSA	Topological polar surface area
TB	Tuberculosis
TRP	Tryptophan
TYR	Tyrosine
VAL	Valine
VDW	Van der Waal interaction
VIF	Variance inflation factor
WHO	World Health Organization

## Introduction

Neglected tropical diseases (NTDs) are a group of infectious diseases which are endemic in developing countries majorly tropics and sub-tropics. Unlike Human Immunodeficiency Virus (HIV)/Acquired immunodeficiency syndrome (AIDS), tuberculosis (TB) and malaria which are receiving greater treatment and research funding, NTDs are truly neglected (Wilsher 2011). According to the World Health Organization (WHO), ailments like human African trypanosomiasis, schistosomiasis, onchocerciasis (river blindness), lymphatic filariasis (elephantiasis), rabies, and buruli cancer are amongst many others classified as NTDs (Hotez et al. 2020). This study is focused on two common filarial diseases; Lymphatic filariasis and onchocerciasis. Lymphatic filariasis is caused by *wuchereria bancrofti*, *Brugia malayi* and *Brugia timori*, while *onchocerca volvulus* is the causative organism for onchocerciasis (Bakowski et al. 2019). Elephantiasis has been reported to cause over 2.8 million disabilities worldwide, whereas river blindness is the global second leading cause of blindness (Jacobs et al. 2019; Cooper and Nutman 2013). Both diseases were equally reported to further aggravate the health of those who

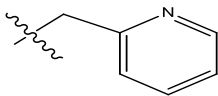
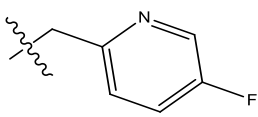
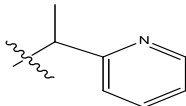
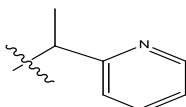
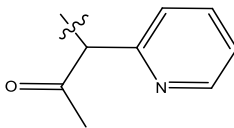
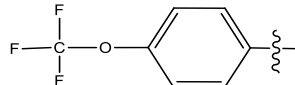
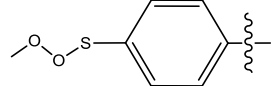
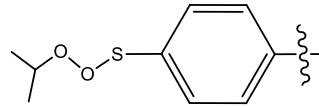
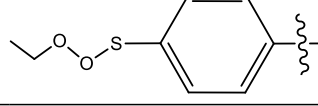
are already down with life-threatening infections like HIV, TB or malaria (McGillan 2017). Elephantiasis is transmitted by a wide range of mosquitoes, while *onchocerca volvulus* is transmitted to its hosts by the blackflies (McGillan 2017).

One specific approach adopted generally over the years to reduce the impact of these filarial infections on the population, is the method of Mass Drug Administration (MDA) (Carter et al. 2020). Notable drugs administered through MDA programs over time include ivermectin, albendazole, and diethyl carbamazepine, either as a dual (annual to bi-annual) or as triple-drug (once every 3 years) treatment (Jacobs et al. 2019; Carter et al. 2020). Unfortunately, the various drugs administered through MDA programs lack enough efficiency to eliminate the adult worms. It is therefore, important to identify new approaches to eliminate adult worms so as to effectively cut down the time frames for both diseases' elimination (Jacobs et al. 2019; Lakshmi et al. 2010). Fortunately, these nematodes causing filarial diseases are said to endosymbiotically co-habit with a gram-negative bacterium called *Wolbachia* (Ugbe et al. 2021). *Wolbachia* is known to be widely distributed and infects a wide range of insects and nematodes species of the phylum arthropod (Kurz et al. 2008). *Wolbachia pipientis* is the strain which is common to nematodes causing filarial diseases (McGillan 2017). The nature of endosymbiotic relationship between *Wolbachia* and infected worm is unclear, it has however been reported that *wolbachia* is important during the embryonic development process in infected nematodes (Townson et al. 2000). It has also been suggested that *wolbachia* can synthesize detoxification enzymes such as catalase, while other reports suggested that the bacteria may play a significant role in nutrition for the host (Henkle-Duhrsen et al. 1998). In the search for new anti-filarial drugs, some researchers have chosen to target *wolbachia*, which past researches have shown that its elimination from the host filarial nematodes leads to antifilarial effects with the reduction of adult worm's lifespan (McGillan 2017; Bouchery et al. 2013). A clinically relevant anti-bacteria drug, doxycycline (Reference drug in this study) has over the years been used for the treatment of lymphatic filariasis and onchocerciasis. However, the treatment method lacks the necessary efficiency to be administered through the MDA owing to its requirement for long treatment periods of about 4–6 weeks, contraindications in pregnancy and in children (McGillan 2017). Therefore, efforts in the development of novel *wolbachia* inhibitors with short treatment periods and reduced complications are important.

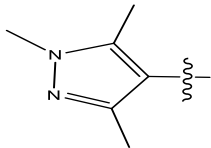
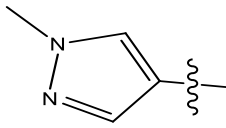
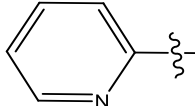
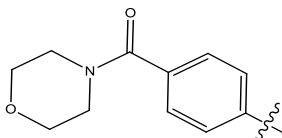
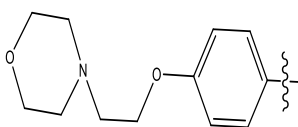
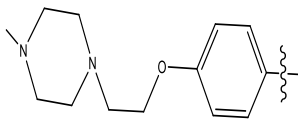
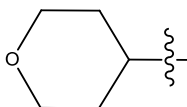
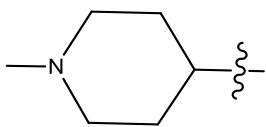
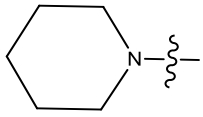
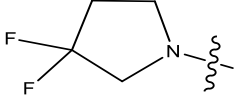
Computational tools play a major role in lead optimization phase of drug discovery (Sliwoski et al. 2014). It saves cost, time and tends to be more effective than the traditional methods (Lawal et al. 2021). The knowledge of Quantitative Structure Activity Relationship (QSAR) helps in establishing a relationship between various molecular structures



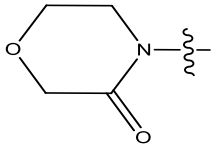
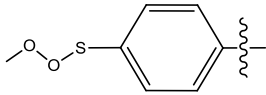
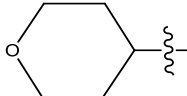
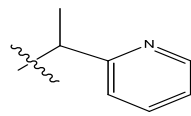
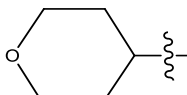
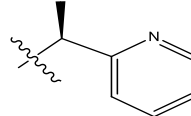
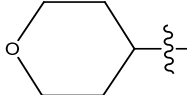
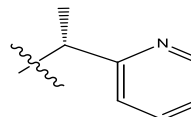
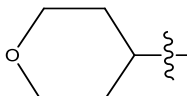
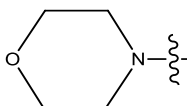
**Table 1** Molecular structures and anti-*wolbachia* activities of pyrazolopyrimidine derivatives

Comp ID	R <sub>1</sub>	R <sub>2</sub>	R <sub>3</sub>	R <sub>4</sub>	R <sub>5</sub>	EC <sub>50</sub> (nM)	pEC <sub>50</sub>
1	H		Phenyl	Isopropyl	H	647	6.1891
2	H	Pyridin-2-ylmethyl	Phenyl	Tert-butyl	H	1854	5.7319
3	H	Benzyl	Phenyl	Methyl	H	3012	5.5211
4	H	2-chlorobenzyl	Phenyl	Methyl	H	5176	5.2860
5	H		Phenyl	Methyl	H	1384	5.8589
6	H	Pyridin-2-ylmethyl	Phenyl	Methyl	H	145	6.8386
7	H		Phenyl	Methyl	Methyl	90	7.0458
8	H		4-fluorophenyl	Methyl	Methyl	93	7.0315
9	H	Pyrimidin-2-ylmethyl	4-fluorophenyl	Methyl	Methyl	33	7.4815
10	H	Pyrazin-2-ylmethyl	4-fluorophenyl	Methyl	Methyl	183	6.7375
11	H	Pyrimidin-4-ylmethyl	4-fluorophenyl	Methyl	Methyl	518	6.2857
12	H		4-fluorophenyl	Methyl	Methyl	456	6.3410
13	methyl	Pyridin-2-ylmethyl	4-fluorophenyl	Methyl	Methyl	2500	5.6021
14	H	Pyridin-2-ylmethyl	4-fluorophenyl	Fused cyclopentane at positions 5 and 6		93	7.0315
15	H	Pyridin-2-ylmethyl	4-fluorophenyl	Methyl	Chloro	51	7.2924
16	H	Pyridin-2-ylmethyl	4-fluorophenyl	Methyl	2,2,2-trifluoroethyl	15	7.8239
17	H	Pyridin-2-ylmethyl	4-chlorophenyl	Methyl	H	674	6.1713
18	H	Pyridin-2-ylmethyl		Methyl	Methyl	664	6.1778
19	H	Pyridin-2-ylmethyl		Methyl	Methyl	143	6.8446
20	H	Pyridin-2-ylmethyl	Benzonitrile	Methyl	Methyl	664	6.1778
21	H	Pyridin-2-ylmethyl	4-chlorophenyl	Methyl	Methyl	84	7.0757
22	H	Pyridin-2-ylmethyl	o-tolyl	Methyl	Methyl	102	6.9914
23	H	Pyridin-2-ylmethyl	methylbenzoate	methyl	methyl	179	6.7471
24	H	Pyridin-2-ylmethyl		Methyl	Methyl	175	6.7570
25	H	Pyridin-2-ylmethyl		Methyl	Methyl	131	6.8827

**Table 1** (continued)

Comp ID	R <sub>1</sub>	R <sub>2</sub>	R <sub>3</sub>	R <sub>4</sub>	R <sub>5</sub>	EC <sub>50</sub> (nM)	pEC <sub>50</sub>
26	H	Pyridin-2-ylmethyl		Methyl	Methyl	1479	5.8300
27	H	Pyridin-2-ylmethyl		Methyl	Methyl	119	6.9245
28	H	Pyridin-2-ylmethyl		Methyl	Methyl	43	7.3665
29	H	Pyridin-2-ylmethyl		Methyl	Methyl	680	6.1674
30	H	Pyridin-2-ylmethyl		Methyl	Methyl	844	6.0737
31	H	Pyridin-2-ylmethyl		Methyl	Methyl	1228	5.9108
32	H	Pyridin-2-ylmethyl	H	Methyl	Methyl	105	6.9788
33	H	Pyridin-2-ylmethyl	Bromo	Methyl	Methyl	176	6.7544
34	H	Pyridin-2-ylmethyl	Chloro	Methyl	Methyl	122	6.9136
35	H	Pyridin-2-ylmethyl	Fluoro	Methyl	Methyl	164	6.7851
36	H	Pyridin-2-ylmethyl	Difluoromethoxy	Methyl	Methyl	251	6.6003
37	H	Pyridin-2-ylmethyl	Fluoromethoxy	Methyl	Methyl	629	6.2013
38	H	Pyridin-2-ylmethyl	Chloro	Methyl	Chloro	311	6.5072
39	H	Pyridin-2-ylmethyl		Methyl	Methyl	52	7.2840
40	H	Pyridin-2-ylmethyl	Tetrahydro-2H-pyran-4-yl	Methyl	Chloro	73	7.1367
41	H	Pyridin-2-ylmethyl		Methyl	Chloro	561	6.2510
42	H	Pyridin-2-ylmethyl		Methyl	Chloro	38	7.4202
43	H	Pyridin-2-ylmethyl		Methyl	Chloro	16	7.7959

**Table 1** (continued)

Comp ID	R <sub>1</sub>	R <sub>2</sub>	R <sub>3</sub>	R <sub>4</sub>	R <sub>5</sub>	EC <sub>50</sub> (nM)	pEC <sub>50</sub>
44	H	Pyridin-2-ylmethyl		Methyl	Chloro	1183	5.9270
45	H	Pyridin-2-ylmethyl	Chloro	H	Methyl	201	6.6968
46	H	Pyridin-2-ylmethyl	4-fluorophenyl	H	Methyl	38	7.4202
47	H	Pyridin-2-ylmethyl		H	Methyl	293	6.5331
48	H	Pyridin-2-ylmethyl		H	Methyl	32	7.4948
49	H			H	Methyl	14	7.8539
50	H			H	Methyl	23	7.6383
51	H			H	Methyl	34	7.4685
52	H	Pyridin-2-ylmethyl		H	Methyl	49	7.3098

three-dimensional (3-D) structural form. The 3-D structures were first optimized geometrically by energy minimization. Thereafter, Molecular Mechanics Force Field (MMFF) was used to minimize their chemical structures in order to remove tension energy of the molecules' conformation. Further optimization was then conducted using Density Functional Theory (DFT) with Becke's three-parameter read-Yang-Parr hybrid (B3LYP) option and utilizing the 6-31G basis set. The thoroughly optimized structures were then saved in SD file format for use in descriptor calculation (Wang et al. 2020; Li et al. 2004).

### Molecular descriptor calculation

The resulting data in SD file format obtained earlier from the optimization process were imported into the Pharmaceutical Data Exploration Laboratory (PaDEL)-descriptor software (version 2.20) to calculate the molecular descriptors for all

fifty two (52) pyrazolopyrimidine derivatives (Lawal et al. 2021).

### Data-set pretreatment and splitting into training and test sets

The pretreatment of the generated descriptor pool was carried out using the Drug Theoretical and Cheminformatics Laboratory (DTC Lab) based software GUI 1.2 so as to remove descriptors which were not informative (Adeniji et al. 2020). The pretreated data were then divided into the modeling train set data and external evaluation test set data in the ratio of 70:30 respectively, with the help of DTC Lab derived software which utilizes the Kennard Stone method for data set division (Kennard and Stone 1969). The splitting of data set into training and test sets was based on the closeness of the representative points of the test set to the representative points of the training set in the multidimensional descriptor space (Ugbe et al. 2021).

## MLR-GFA model building

The Genetic Function Approximation (GFA) as a statistical technique in the Material Studio software (version 8.0) was used to generate the models based on Multi-Linear Regression (MLR) approach. GFA was used to obtain the optimum descriptor combinations constituting the QSAR models, while MLR helps to establish the relationship between the biological activities,  $pEC_{50}$  (dependent variable) and the molecular descriptors (independent variables) (Arthur et al. 2020). The Multi-linear regression equation assumes the following form (Eq. 2) (Adawara et al. 2020):

$$Y = k_1x_1 + k_2x_2 + k_3x_3 + \dots C \quad (2)$$

where Y represents the dependent variable; 'k's and 'x's represent respectively regression coefficients and independent variables; 'C' equals intercept or regression constant.

## Assessment of model quality (internal validation)

Internal validation assessment of the built models was carried out on Material studio by GFA approach using the Friedman formula, correlation coefficient ( $R^2$ ) and cross validation coefficient ( $Q^2_{cv}$ ). Determination of the Friedman Lack-Of-Fit (LOF) allows for the best fitness score to be obtained. LOF is defined as follows (Eq. 3):

$$LOF = \frac{SEE}{\left(1 - \frac{c+dxp}{M}\right)^2} \quad (3)$$

where: SEE is the Standard Error of Estimation (SEE), with low values indicating high quality model. SEE is defined thus (Eq. 4):

$$SEE = \sqrt{\frac{(Y_{exp} - Y_{pred})^2}{N - P - 1}} \quad (4)$$

c represents number of terms in the model, d is a user-defined smoothing parameter, p is total number of descriptors in the model while M equals the number of data in the training set (Adeniji et al., 2018).

Another important parameter, the correlation coefficient ( $R^2$ ) measures the degree of fitness of the regression equation.  $R^2$  value closer to 1 is an indicative of high quality model.

$R^2$  is a commonly used internal validation parameter and is expressed thus (Eq. 5):

$$R^2 = 1 - \left[ \frac{\sum (Y_{exp} - Y_{pred})^2}{\sum (Y_{exp} - \bar{Y}_{training})^2} \right] \quad (5)$$

where:  $\bar{Y}_{training}$ ,  $Y_{exp}$ , and  $Y_{pred}$  equal respectively, the mean  $pEC_{50}$ , experimental activity and the predicted activity in the training set.

$R^2$  is usually adjusted in order to afford the model stability and reliability because it directly varies with increase in number of descriptors. The adjusted  $R^2$  is defined thus:

$$R^2_{adj} = \frac{R^2 - p(n - 1)}{n - p + 1} \quad (6)$$

where: p is the number of descriptors in the model, and n equals the number of compounds in the training set.

Another important parameter is the leave-one-out (LOO) cross-validation regression coefficient ( $Q^2_{cv}$ ), which determines the ability of a built QSAR model to predict the activity of new compounds. A high value of  $Q^2_{cv}$  indicates a high internal predictive power and a good robustness of the QSAR model.  $Q^2_{cv}$  is defined as follows (Eq. 7):

$$Q^2_{cv} = 1 - \left[ \frac{\sum (Y_{pred} - Y_{exp})^2}{\sum (Y_{exp} - \bar{Y}_{training})^2} \right] \quad (7)$$

$Y_{exp}$  and  $Y_{pred}$  represent the experimental activity and predicted activity in the training set respectively.  $\bar{Y}_{training}$  equals the average  $pEC_{50}$  in the training set.

## Assessment of model quality (external validation)

The model's predictive power was assessed externally to show if the model could predict the activity values of the test set compounds. The predictive strength of the model depends on the value of the predicted  $R^2$  ( $R^2_{test}$ ) defined thus (Eq. 8) (Isyaku et al. 2020):

$$R^2_{test} = 1 - \frac{\sum (Y_{pred_{test}} - Y_{exp_{test}})^2}{\sum (Y_{pred_{test}} - \bar{Y}_{training})^2} \quad (8)$$

$Y_{pred_{test}}$  = predicted activity of test set,  $Y_{exp_{test}}$  = experimental activity of test set,  $\bar{Y}_{training}$  = mean value of experimental activity of the training set.

Furthermore, the data was subjected to the Golbraikh and Tropsha acceptable model criteria using the MLRplus Validation tool (version 1.3) as follows (Roy et al. 2013; Edache et al. 2020).

$$|r_o^2 - r_o'^2| \text{ (Threshold value } < 0.3).$$

$$|r^2 - \frac{r_o^2}{r^2}| \text{ (Threshold value } < 0.1).$$

$$k' \text{ (threshold value } 0.85 \leq k \leq 1.15).$$

where:  $r^2$  = square correlation coefficients of the plot of experimental activity versus predicted activity values.



$r_o^2$  = square correlation coefficients of the plot of experimental activity versus predicted activity values at zero intercept.  $r'_o^2$  = square correlation coefficients of the plot of predicted activity versus experimental activity at zero intercept.  $k'$  = slope of the plot of predicted activity against experimental activity at zero intercept.

### Y-randomization test

The Robustness of the built QSAR model was assessed by Y-randomization technique in which MLR models are generated by randomly shuffling the dependent variable while keeping the independent variables constant (Adawara et al. 2020). This is for a confirmation that the QSAR model built is strong and not created by chance. A low  $R^2$  and  $Q^2$  values for several iteration indicates a good applicability of the built model. The coefficient of determination ( $cR_p^2$ ) is defined as follows (Eq. 9):

$$cR_p^2 = RX \left[ R^2 - (R_r)^2 \right]^2 \quad (9)$$

where:  $cR_p^2$  = Y-randomization coefficient,  $R$  = correlation coefficient for Y-Randomization,  $R_r$  = average 'R' of random models.  $cR_p^2$  value greater than 0.50 is a requirement for the model to pass Y-randomization test.

### Statistical analysis of the descriptors

#### Mean effect (ME)

The mean effect (ME) value shows the relative contribution of each descriptor in a model, defined as (Eq. 10):

$$ME = \frac{B_j \sum_i^n D_j}{\sum_j^m (B_j \sum_i^n D_j)} \quad (10)$$

where:  $\beta_j$  is the coefficient of the descriptor  $j$  in the model,  $D_j$  is the value of each descriptor in the data matrix for each molecule in the training set,  $m$  is the number of the descriptor that appears in the model,  $n$  is the number of molecules in the training set (Abdullahi et al. 2019).

#### Variance inflation factor (VIF)

The degree of multi-co-linearity or correspondence between the descriptors is measured by the Variance Inflation Factor (VIF), usually defined as (Eq. 11):

$$VIF = \frac{1}{(1 - R^2)} \quad (11)$$

where:  $R^2$  is the correlation coefficient of the multiple regression between the variables within the model. VIF value of 1 indicates no inter-correlation exists for each variable, for VIF in the range of 1–5, the related model is acceptable; and if VIF is greater than 10, the related model is unstable and unacceptable (Abdullahi et al. 2019).

### Evaluation of the model applicability domain

Evaluating the applicability domain (AD) of a QSAR model is important to ascertain the reliability and robustness of the built QSAR model. AD provides one the chance to estimate the uncertainty in the prediction of compounds based on their similarity with the training set compounds, used in the model building (Tropsha et al. 2003). The leverage approach was used to describe the AD of the developed model. The leverage ( $h$ ) of a particular chemical compound is defined thus (Eq. 12):

$$h = X(X^T X)^{-1} X^T \quad (12)$$

where:  $X = m \times k$  descriptor matrix of the training set compound,  $X^T$  = transpose matrix of  $X$ .

The warning leverage ( $h^*$ ) which is the range of values used to check for influential molecule or outlier is defined below (Eq. 13):

$$h^* = 3 \frac{(j + 1)}{m} \quad (13)$$

where:  $m$  = number of training set compounds,  $j$  = number of descriptors in the model.

A plot of the standardized residuals against leverages otherwise called the William's plot was used to evaluate the significant area in the model's chemical space. As a rule, compounds which fall within this area on the plot are the approved predicted compounds (Adeniji et al. 2020; Veerasamy et al. 2011).

### Ligand based drug design

The ligand based drug design approach was adopted in designing Six (6) new pyrazolopyrimidine analogues basically by deletion, substitution and insertion of substituent(s) into the template structure (43) based on the information provided by the molecular descriptors (Majorly GATS2v, GATS6s, ATSC4e and GATS8s) (Adeniji et al. 2020). The newly designed compounds and reference drug used in this study (doxycycline) were prepared in four steps as earlier reported under 'molecular geometry optimization' section; drawing of chemical structures, energy minimization, minimization by MMFF, and optimization by DFT approach.



## Prediction of pharmacokinetic properties

Pharmacokinetics properties prediction constitute an absolutely necessary stage in drug discovery's early phase because only molecules with good drug-likeness properties and excellent ADMET profiles advance into the pre-clinical research phase (Lawal et al. 2021). Hence, Two (2) pyrazolopyrimidine derivatives (**16** and **43**) with better inhibitory activities and lower residual values alongside the newly designed compounds (**A1–A6**) were investigated for their drug-likeness and ADMET properties using the online web servers; <http://www.swissadme.ch/index.php> and <http://biosig.unimelb.edu.au/pkcsms> respectively. The Lipinski's rule of five (RO5) is a widely used criterion for oral bioavailability. Hence, the tested compounds would be assessed for oral bioavailability using the RO5 criteria (Lipinski et al. 2001).

## Molecular docking study

The newly designed compounds and the reference drug (doxycycline) were docked onto the receptor (OTU deubiquitinase)'s binding pocket using the iGEMDOCK software, while using Biovia Discovery Studio Visualizer to analyze the resulting protein–ligand interaction profiles (Ibrahim et al. 2021; Kumar et al. 2016).

## Results and discussion

### QSAR study

A theoretical study (QSAR) was conducted on fifty two (52) pyrazolopyrimidine derivatives, in order to establish a quantitative relationship between their structures and their anti-*wolbachia* activities. The built models were subjected to both internal and external validation tests, in which model 3 (Eq. 14) best satisfied the requirement for a good QSAR model. Table 2 described the various descriptors used in the model, while the experimental and predicted activity values

together with their residual values for pyrazolopyrimidine derivatives were presented in Table 3. Also, the predicted activity values were plotted against those of experimental activity for both training and test sets and presented in Fig. 2. A further plot of standardized residual against experimental activities was obtained and presented in Fig. 3. In order to ascertain the stability, robustness, reliability and predictive power of the built QSAR model, internal and external validation tests were conducted, and the results presented in Table 4.

A combined GFA and MLR approaches led to the selection of seven (7) descriptors, and generation of four (4) QSAR models respectively. Model 3 (Eq. 14) was found to best satisfied the requirement for a reliable QSAR model. The low residual values between the experimental and predicted activities as shown in Table 3 imply that the model has a high predictive strength. The  $R^2$  values of 0.8104 and 0.750 for training set and test set respectively as obtained from Fig. 2 compare perfectly well with those obtained from GFA (0.8104 and 0.7501) and MLRplusValidation analysis (0.8104 and 0.7501) as reported in Table 4. The grouping together of points along the line of best fit in Fig. 2 shows that the experimental and predicted activity values are well correlated, indicating that the built model is reliable and robust. The random spread of standardized residuals on both sides of zero in Fig. 3 is an indication that the built model is free of any systematic error.

$$\begin{aligned}
 pEC_{50} = & -1.067945613 * ATSC4e \\
 & - 4.379278216 * AATSC4s \\
 & + 4.035879647 * GATS2v \\
 & + 0.922556367 * GATS8e \\
 & + 1.109246296 * GATS6s \\
 & - 0.097883280 * nsSeH \\
 & + 0.696906031 * SssSnH2 \\
 & - 0.253197268
 \end{aligned} \tag{14}$$

Additionally, Pearson's correlation statistical analyses were performed on the values of all seven descriptors in

**Table 2** Selected descriptors used in the QSAR model

S/no	Descriptor symbol	Description	Class
1	ATSC4e	Centred Broto-Moreau autocorrelation of lag 4 weighted by Sanderson electronegativity	2D
2	AATSC4s	Average centered Broto-Moreau autocorrelation—lag 4/weighted by I-state	2D
3	GATS2v	Geary autocorrelation—lag2/weighted by van der waals volume	2D
4	GATS8e	Geary autocorrelation of lag 8 weighted by Sanderson electronegativity	2D
5	GATS6s	Geary autocorrelation of lag 6 weighted by I-state	2D
6	nsSeH	Count of atom-type E-State	2D
7	SssSnH2	Sum of atom-type E-State	2D

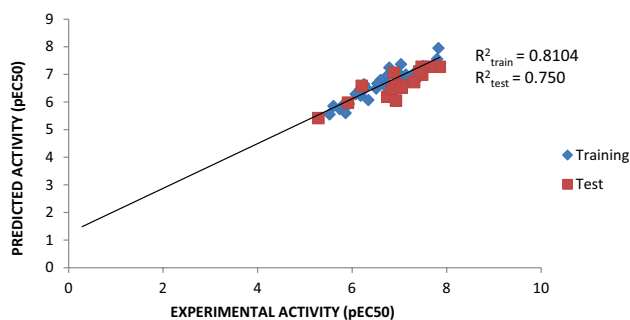
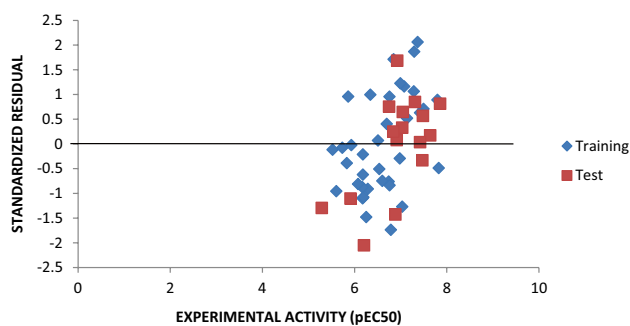
**Table 3** Experimental, predicted and residual values of pyrazolopyrimidine derivatives

Compound ID	Exp. pEC <sub>50</sub>	Pred. pEC <sub>50</sub>	Residuals
1	6.189096	6.475834	-0.28674
2	5.73189	5.751861	-0.01997
3	5.521145	5.551556	-0.03041
*4	5.286006	5.419773	-0.13377
5	5.858864	5.603058	0.255806
*6	6.838632	6.452273	0.386359
*7	7.045757	6.526182	0.519576
*8	7.031517	6.618447	0.41307
*9	7.481486	6.98818	0.493306
10	6.737549	6.939861	-0.20231
11	6.28567	6.527686	-0.24202
12	6.341035	6.075156	0.265879
13	5.60206	5.855867	-0.25381
14	7.031517	7.368888	-0.33737
15	7.29243	6.795143	0.497287
16	7.823909	7.953198	-0.12929
17	6.17134	6.463977	-0.29264
18	6.177832	6.233958	-0.05613
19	6.844664	6.388609	0.45606
20	6.177832	6.342709	-0.16488
21	7.075721	6.765542	0.310179
22	6.9914	6.664351	0.327049
*23	6.747147	6.191564	0.555583
24	6.756962	6.979128	-0.22217
*25	6.882729	7.061255	-0.17853
26	5.830032	5.933092	-0.10306
*27	6.924453	6.055529	0.868924
28	7.366532	6.817488	0.549044
29	6.167491	6.400326	-0.23283
30	6.073658	6.288886	-0.21523
*31	5.910802	5.980347	-0.06955
32	6.978811	7.056629	-0.07782
33	6.754487	6.4994	0.255087
*34	6.91364	6.585139	0.328501
35	6.785156	7.247238	-0.46208
36	6.600326	6.799095	-0.19877
*37	6.201349	6.589389	-0.38804
38	6.50724	6.487985	0.019255
39	7.283997	7.00048	0.283517
40	7.136677	6.998007	0.13867
41	6.251037	6.644402	-0.39336
*42	7.420216	7.105898	0.314319
43	7.79588	7.55812	0.23776
44	5.927015	5.932727	-0.00571
45	6.696804	6.588648	0.108156
46	7.420216	7.251703	0.168513
47	6.533132	6.667723	-0.13459
48	7.49485	7.305925	0.188925
*49	7.853872	7.278034	0.575837

**Table 3** (continued)

Compound ID	Exp. pEC <sub>50</sub>	Pred. pEC <sub>50</sub>	Residuals
*50	7.638272	7.278034	0.360238
*51	7.468521	7.278034	0.190487
*52	7.309804	6.722164	0.58764

Key: \*-test set compound, EC<sub>50</sub>- half-maximal effective concentration

**Fig. 2** Plot of predicted pEC<sub>50</sub> against Experimental pEC<sub>50</sub> for training and test sets**Fig. 3** Plot of standardized residual against experimental pEC<sub>50</sub> for training and test sets

the built QSAR Model and the results were reported in Table 5. Another significant validation test is the Y-Randomization test, which was also performed and the result presented in Table 6. The low correlation coefficients (less than 0.50) which exist between each descriptor in the built model (Table 5) indicate no inter-correlation between each descriptor. The Variance Inflation Factor (VIF) for all 7 descriptors has values ranging from 1 – 5, an indication of the stability and acceptability of the built model (Table 5). The absolute t-statistics of each descriptor is greater than 2, showing that the selected descriptors were good (Adeniji et al. 2018). Also, Table 5 shows that the evaluated p-values at 95% confidence level for all descriptor were less than 0.05. This means that the alternative hypothesis which posits that there is a relationship between inhibitory activities and the descriptors holds. Additionally, the values of the Mean

**Table 4** Validated parameters of the QSAR model

Validation parameters	Model	QSAR validation standard
	Training set	
Friedman LOF	0.4123	–
R-squared ( $R^2$ )	0.8104	$\geq 0.6$
Adjusted R-squared ( $R^2_{adj}$ )	0.7629	–
Cross validated R-squared ( $Q^2_{cv}$ )	0.6981	$\geq 0.5$
$R^2 - Q^2_{cv}$	0.1123	$\leq 0.3$
Significant Regression	YES	–
Significance-of-regression F-value	17.0924	–
Critical SOR F-value (95%)	2.3672	–
Replicate points	0	–
Computed experimental error	0.0000	–
Lack-of-fit points	28	–
Min expt. error for non-significant LOF (95%)	0.2447	–
	Test set	
R-squared ( $R^2_{test}$ ) i.e. $r^2$	0.7501	$\geq 0.6$
Number of test set compounds ( $N_{test\ set}$ )	16	$\geq 5$
$ r^2_o - r'^2_o $	0.10742	$< 0.3$
$ r^2 - \frac{r^2_o}{r^2} $	0.00123	$< 0.1$
k	1.04568	$0.85 < k < 1.15$

**Table 5** Pearson's correlation and statistical analyses of descriptors used in the QSAR model

Inter-correlation							
	ATSC4e	AATSC4s	GATS2v	GATS8e	GATS6s	nsSeH	SssSnH2
ATSC4e	1						
AATSC4s	0.525345	1					
GATS2v	0.307996	0.028935	1				
GATS8e	0.478104	0.241975	– 0.12161	1			
GATS6s	0.62834	0.558828	0.260268	0.258477	1		
nsSeH	– 0.13871	0.184628	– 0.43041	– 0.03379	0.147126	1	
SssSnH2	0.039192	0.270547	– 0.04425	0.106862	0.24912	0.310204	1
Statistical parameters							
VIF	2.630942	1.737761	1.631929	1.496797	2.174509	1.558148	1.229976
ME	0.138695	0.035656	0.518466	0.115025	0.15305	– 0.05164	0.090747
Coefficients	– 1.0679	– 4.3793	4.035879	0.922556	1.10925	– 0.09788	0.69691
Std. Error	0.181153	1.285964	1.23684	0.274962	0.268721	0.028934	0.127429
t Stat	– 5.8953	– 3.40544	3.263056	3.355218	4.127868	– 3.38294	5.468995
p-value	2.40E–06	0.002014	0.002901	0.002292	0.000298	0.002134	7.71E–06

Effect (ME) reported in Table 5 provide vital information on the effect and degree of each descriptor's contributions in the model. The magnitudes and signs of ME values signify their respective strength and direction on the molecules' inhibitory activities. All the descriptors except *nsSeH* have positive ME, indicating that increasing or decreasing their

values will lead to a corresponding increase or decrease in the anti-proliferative activities respectively. Increasing the values of *nsSeH* on the other hand will lead to a decrease in the anti-*wolbachia* activities. GATS2V with the highest ME value has the greatest influence on the molecules' inhibitory activities. GATS2v which is the Geary autocorrelation—lag

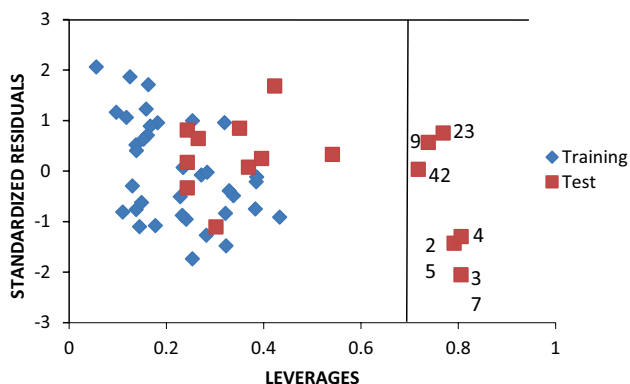
**Table 6** Y-Randomization test parameters

Model	R	R <sup>2</sup>	Q <sup>2</sup>
Original	0.900199	0.810358	0.698051
Random 1	0.218226	0.047622	-0.58138
Random 2	0.410592	0.168586	-0.39194
Random 3	0.292327	0.085455	-0.66299
Random 4	0.307793	0.094737	-0.54198
Random 5	0.322781	0.104187	-0.41129
Random 6	0.471172	0.222003	-0.41909
Random 7	0.358435	0.128476	-0.36971
Random 8	0.38892	0.151258	-0.41459
Random 9	0.278492	0.077558	-0.72302
Random 10	0.423864	0.179661	-0.58126
Random models parameters			
Average r	0.34726		
Average r <sup>2</sup>	0.125954		
Average Q <sup>2</sup>	-0.50973		
cRp <sup>2</sup>	0.747636		

2/weighted by van der Waals volumes, which has a positive ME is suggested to contribute positively to anti-wolbachia activity. It measures the strength of the relationship between van der Waals volumes of two atoms in a molecule that are two bond apart (Adawara et al. 2020).

The low values of R<sup>2</sup> and Q<sup>2</sup> obtained from the random reshuffling (Table 6) inferred that the built model is stable, robust and reliable. The value of coefficient for Y-randomization, cR<sup>2</sup>p (0.747636) greater than 0.50, supports the claim that the built model is powerful and not inferred by chance.

The scatter plot of the standardized residuals versus the leverages (William's Plot) obtained to ascertain the model's applicability domain is as shown in Fig. 4. The William's plot clearly shows that all the compounds falls within the square area  $\pm 3$  of standardized cross-validated residual. It can therefore be inferred that no outlier is present in the data

**Fig. 4** The plot of standardized residuals against the leverage values (William's plot)

set. However, eight compounds (2, 3, 4, 5, 7, 9, 23 and 42) were found with leverage values greater than the calculated warning leverage ( $h^* = 0.67$ ), and are said to be influential molecules.

Consequently, compounds **16** and **43** with relatively higher predicted inhibitory activities of 7.953 and 7.558 respectively (Table 3), having also contained within the model's applicability domain space (Fig. 4), were subjected to drug-likeness test for possible selection as lead molecule for designing new prominent analogues.

### Ligand-based drug design

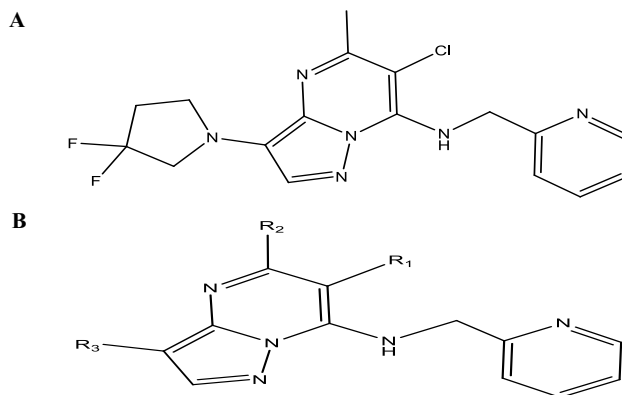
The molecular structure of the lead compound (**43**) and the structural template are presented in Fig. 5A, B, while predicted activities of the newly designed compounds are presented in Table 7.

One of the objectives of the ligand-based design is to be able to design new molecules with better inhibitory activities than their template molecule. Here, the predicted pEC<sub>50</sub> values of the designed compounds were higher than that of the template molecule (**43**) in the order: **A4** (8.9601) > **A1** > **A6** > **A5** > **A3** > **A2** > **43** (7.5581) as shown in Table 7. It therefore affirmed that the various structural modifications of the template structure were based on the information provided by the molecular descriptors in the built QSAR model.

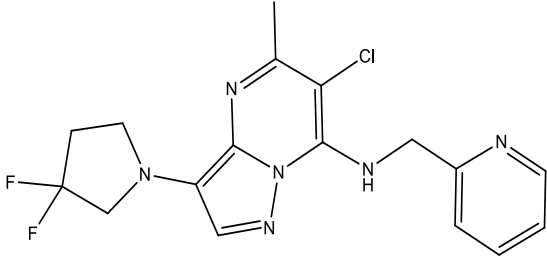
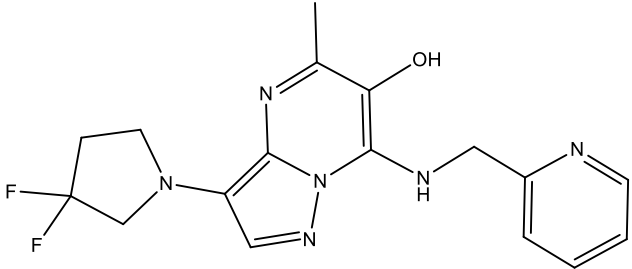
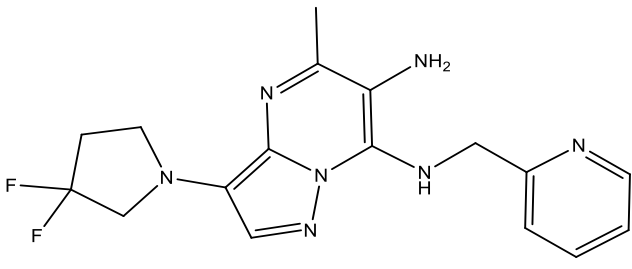
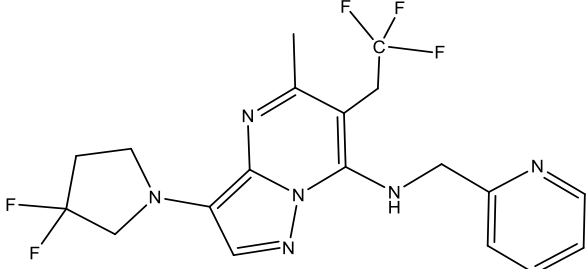
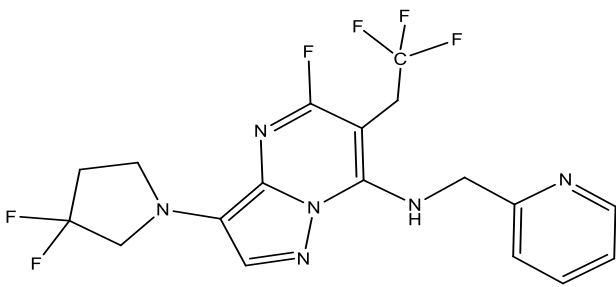
### Pharmacokinetics properties prediction

Results of the pharmacokinetics investigation conducted on **16**, **43** and the six (6) newly designed compounds were presented in Table 8, 9, while Fig. 6a, b shows the oral bio-availability radar of **16** and **43**.

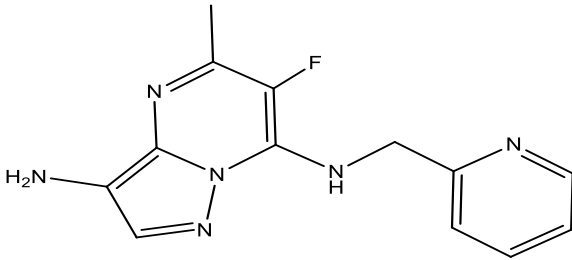
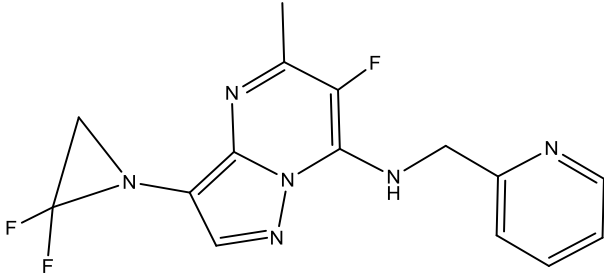
The Lipinski's rule for oral-bioavailability states that a drug molecule is more likely to have poor absorption or permeation when it has Hydrogen Bond Donors (HBD)

**Fig. 5** A Molecular structures of the lead compound B Structural template for the ligand-based design

**Table 7** Predicted pEC<sub>50</sub> of the newly designed pyrazolopyrimidine compounds

Compound ID	Molecular structure	Predicted pEC <sub>50</sub>
Template (43)		7.5581
A1		8.1887
A2		7.7178
A3		7.7894
A4		8.9601

**Table 7** (continued)

Compound ID	Molecular structure	Predicted pEC <sub>50</sub>
A5		7.9997
A6		8.0403

**Table 8** Predicted drug-likeness properties of selected and newly designed compounds

Comp ID	MW (g/mol)	TPSA (Å <sup>2</sup> )	MLOGP	Log S (ESOL)	HBD	HBA	RO5	PAINS	Brenk	SA
16	415.39	55.11	3.88	-5.44	1	7	0	0	0	3.27
43	378.81	58.35	2.67	-4.28	1	5	0	0	0	3.07
A1	360.36	78.58	1.64	-3.54	2	6	0	0	0	3.11
A2	359.38	84.37	1.64	-3.33	2	5	0	0	0	3.10
A3	426.39	58.35	2.97	-4.85	1	8	0	0	0	3.32
A4	430.35	58.35	3.12	-4.90	1	9	0	0	0	3.38
A5	272.28	81.13	1.32	-2.46	2	4	0	0	0	2.73
A6	334.30	58.12	2.08	-3.54	1	6	0	0	2	2.97

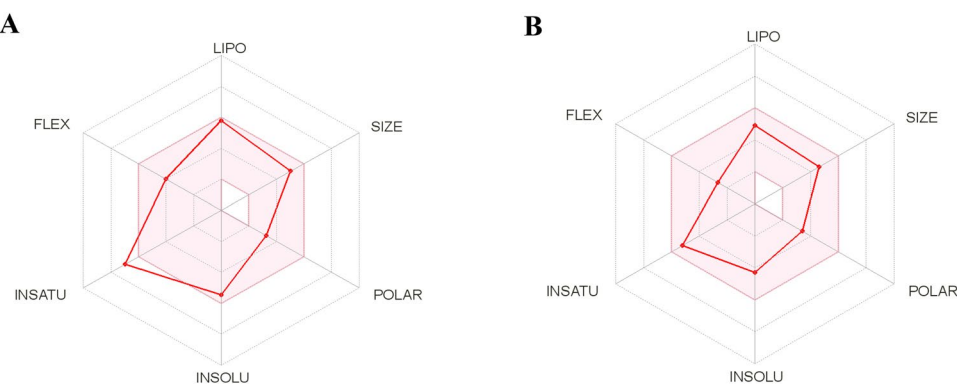
MW-molecular weight, TPSA-topological polar surface area, ESOL-estimated solubility, HBD-hydrogen bond donors, HBA-hydrogen bond acceptors, RO5-Lipinski rule of five violation, SA-synthetic accessibility score

**Table 9** Predicted ADMET properties of the newly designed compounds

Comp ID	Absorption		Distribution		Metabolism				Excretion	Toxicity	
	HIA (%)	Skin LogKp	BBB LogBB	CNS LogPS	CYP3A4		CYP2D6		Total clearance	AMES	MRTD
					S	I	S	I			
A1	95.466	-2.741	-0.902	-3.104	NO	NO	NO	NO	0.032	NO	0.105
A2	95.798	-2.737	-0.854	-3.105	NO	NO	NO	NO	-0.006	NO	0.090
A3	93.318	-2.908	0.142	-3.00	YES	NO	NO	NO	-0.015	NO	-0.344
A4	92.762	-2.894	0.003	-3.049	YES	NO	NO	NO	-0.523	NO	-0.276
A5	96.258	-2.782	-0.595	-3.069	NO	NO	NO	NO	-0.042	NO	0.145
A6	95.801	-2.864	0.170	-3.063	YES	NO	NO	NO	-0.225	NO	-0.159

BBB blood brain barrier, CNS central nervous system, HIA human intestinal absorption, Skin skin permeability, LogBB logarithmic ratio of brain to plasma drug concentration, LogPS blood-brain permeability-surface area product, CYP3A4 cytochrome p450 isoform, CYP2D6 cytochrome p450 isoform, S substrate, I inhibitor, MRTD maximum recommended tolerated dose

**Fig. 6** **A** Oral bioavailability radar of 16; **B** Oral bioavailability radar of 43



of greater than 5, Hydrogen Bond Acceptors (HBA) > 10, Molecular Weight (MW) > 500, and lipophilicity (MLOGP > 4.15 or WLOGP > 5) (Lipinski et al. 2001). Molecules that satisfy at least three out of the four requirements are said to obey the Lipinski's rule for oral-bioavailability (Lawal et al. 2021). As shown in Table 8, all tested molecules perfectly obeyed the Lipinski's rule by showing no violation. Also, the reported values of Topological Polar Surface Area (TPSA) for all molecules are less than 140 Å<sup>2</sup>. Additionally, the synthetic accessibility scores of all tested molecules are in the easy portion (< 5.00), indicating easy laboratory synthesis. Notwithstanding the relatively higher inhibitory activity of compound 16, ligand 43 was the preferred lead molecule, because it possessed a more suitable physico-chemical properties for oral bioavailability as shown from the oral bioavailability radar in Fig. 5. The estimated water solubility (Log S) ranges from moderately soluble (16, 43, A3 and A4) to soluble (A1, A2, A5 and A6). All compounds showed no pains and brek alerts except A6 which showed 2 structural alerts due to the presence of N – C – Halogen and 3-membered heterocycle moieties.

The predicted ADMET properties in Table 9 showed that, the Human Intestinal Absorption (HIA) was high (> 90%) for all newly designed compounds. Skin permeability is a significant consideration for the development of transdermal drug delivery. A skin permeability constant LogKp of greater than – 2.50 is an indication of low skin permeability. Consequently, all the newly designed compounds have LogKp of less than – 2.50, showing good skin penetration ability. Also, all the tested compounds are non-substrates of P-glycoprotein, an enzyme which acts as a biological barrier by extruding toxins and xenobiotics, including drugs out of cells, while A3 and A4 are inhibitors of both P-glycoprotein I and II, indicating that these molecules may easily mediate to reach their target sites with little or no resistance from P-glycoprotein. For a drug molecule to penetrate the Blood–Brain Barrier (BBB) and Central Nervous System (CNS), it is recommended that the logarithmic ratio of brain to plasma drug concentration (logBB) be greater than -1 and the blood–brain permeability-surface area product (logPS)

be greater than -3 respectively. Consequently, all the newly designed compounds showed logBB of greater than – 1, an indication that these molecules cross the BBB. However, all the molecules showed very poor CNS permeability i.e. logPS < – 3. Furthermore, Cytochrome P450 enzymes are important detoxification enzymes in the body which oxidize xenobiotics to facilitate their excretion. The two major isoforms responsible for drug metabolism, CYP-3A4 and CYP-2D6 were reported. Only A3, A4 and A6 are substrates of CYP-3A4. No substrates of CYP-2D6 and no inhibitors of CYP-3A4 and CYP-2D6. The degree of drug elimination from the body is measured by the drug's total clearance, which is within the accepted range for these newly designed compounds. All molecules showed a negative AMES toxicity, indicating that they are non-mutagenic and cannot act as carcinogen. Additionally, the predicted values of Maximum Recommended Tolerated Dose (MRTD) for all molecules were included in Table 9. MRTD value of less than or equal to 0.477 log (mg/kg/day) is considered low, and high if greater than 0.477 log (mg/kg/day). The overall drug-likeness and ADMET properties showed good pharmacokinetic profiles for these molecules. Therefore, the newly designed molecules except A6 (with 2 structural alerts) could be considered as potential drug candidates for the treatment of lymphatic filariasis and onchocerciasis.

### Molecular docking study

The 3D structures of the receptor and ligand A1 were presented in Fig. 7A, B; while results of the docking study conducted between the target receptor (OTU deubiquitinase) (Fig. 8), the newly designed compounds, and the reference drug doxycycline (Fig. 7) were presented in Table 10 and Figs. 9, 10, 11, 12, 13, 14, 15.

All tested molecules bind well into the target site cavity in the order; A1 (87.32 kcal/mol) > A3 > A6 > A2 > A4 > doxycycline > A5 (– 78.70 kcal/mol) as reported in Table 10 and Figs. 9, 10, 11, 12, 13, 14, 15, indicating that the newly designed compounds with the exception of A5 bind more strongly to the protein target (OTU deubiquitinase) than



**Fig. 7** **A** 3D structure of prepared receptor (OTU deubiquitinase) **B** 3D structure of prepared ligand (**A1**)

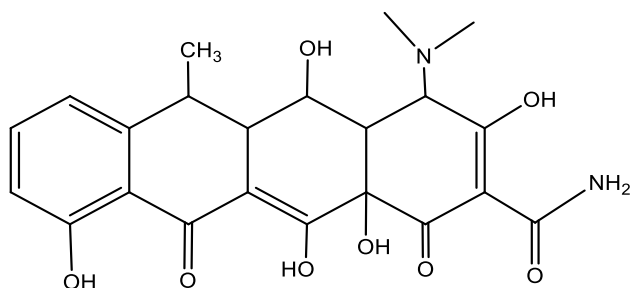
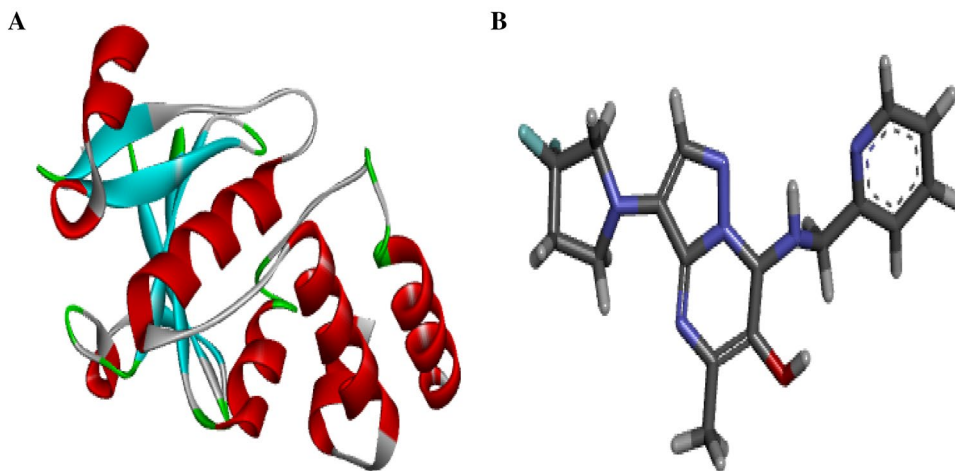


**Fig. 8** Molecular structures of doxycycline

the reference drug doxycycline. As seen from Table 10 and Fig. 9–15, **A1** was observed to have interacted well with the binding site of the OTU deubiquitinase receptor through five (5) conventional hydrogen bonds, one (1) carbon-hydrogen bond and one (1)  $\pi$ -donor hydrogen bond. The hydrophobic interactions include one (1)  $\pi$ -anion, four (4)  $\pi$ -alkyl, one (1) alkyl, two (2)  $\pi$ - $\pi$  T-shaped, and one (1) halogen interactions. The hydroxyl group on the pyrimidine ring system formed 3 conventional hydrogen bonds; two with ASP-177 at distances of 2.55 Å and 2.77 Å, and one with ASP-175 at a distance of 3.30 Å. The Nitrogen atom of the pyrazole ring system and the linker Nitrogen between the pyrimidine and pyridine ring systems formed one conventional Hydrogen bond each with VAL-174 at distances of 3.10 Å and 2.68 Å respectively. Other hydrogen bond interactions are carbon hydrogen bond with LYS-173 at a distance of 3.30 Å and  $\pi$ -donor hydrogen bond with TYR-176 at a distance of 2.86 Å. Also observed was a halogen interaction between one of the fluoro groups on the pyrrolidine ring system and ASN-36 at a distance of 3.69 Å. Others are hydrophobic interactions with PRO-39 (alkyl and  $\pi$ -alkyl), LYS-173 ( $\pi$ -alkyl), TYR-176 ( $\pi$ - $\pi$  T-shaped) and ASP-175 ( $\pi$ -anion).

In general, the various ligands were observed to make very close contacts with great number of amino acid residues including Hydrogen bonding and hydrophobic interactions,

which are two very significant interaction types in drug-receptor binding as shown in Figs. 9, 10, 11, 12, 13, 14, 15. Unlike the newly designed compounds with a fair combination of both hydrogen bonding and hydrophobic interactions with the receptor, the interactions of doxycycline with the target protein were predominantly hydrogen bonding, and having only one hydrophobic interaction ( $\pi$ -anion) with the aspartic acid group (ASP) at position 116 of the target receptor. Imberty et al. (1991) reported that hydrogen bond can be classified as strong or weak based on the distance between hydrogen donor and hydrogen acceptor ( $dis_{(D-A)}$ ) as follows;  $2.5 \text{ \AA} < dis_{(D-A)} < 3.1 \text{ \AA}$  (strong hydrogen bond) and  $3.1 \text{ \AA} < dis_{(D-A)} < 3.55 \text{ \AA}$  (weak hydrogen bond). Consequently, most of the Hydrogen bond distances of the new compounds with the receptor, indicate strong Hydrogen bond interactions with the respective amino acid residues, while doxycycline showed weak hydrogen bond interactions with threonine (THR) at position 109, serine (SER) at position 121 and ASP at position 116. This clearly indicates how well the newly designed compounds bind with OTU deubiquitinase, an essential protein for the survivability of bacteria *Wolbachia*.

## Conclusions

In this study, four (4) QSAR models were developed with a series of fifty two (52) pyrazolopyrimidine derivatives as anti-*wolbachia* agents, amongst which Model 3 best satisfied the requirement for both internal and external validation tests. The model was used to excellently predict the anti-*wolbachia* activities of the various compounds, including the newly designed analogues. Compound **43** was selected as lead molecule ahead of compound **16** as a result of its relatively better drug-likeness properties. All the newly designed compounds showed good pharmacokinetic properties with no violation of the Lipinski's RO5, are orally

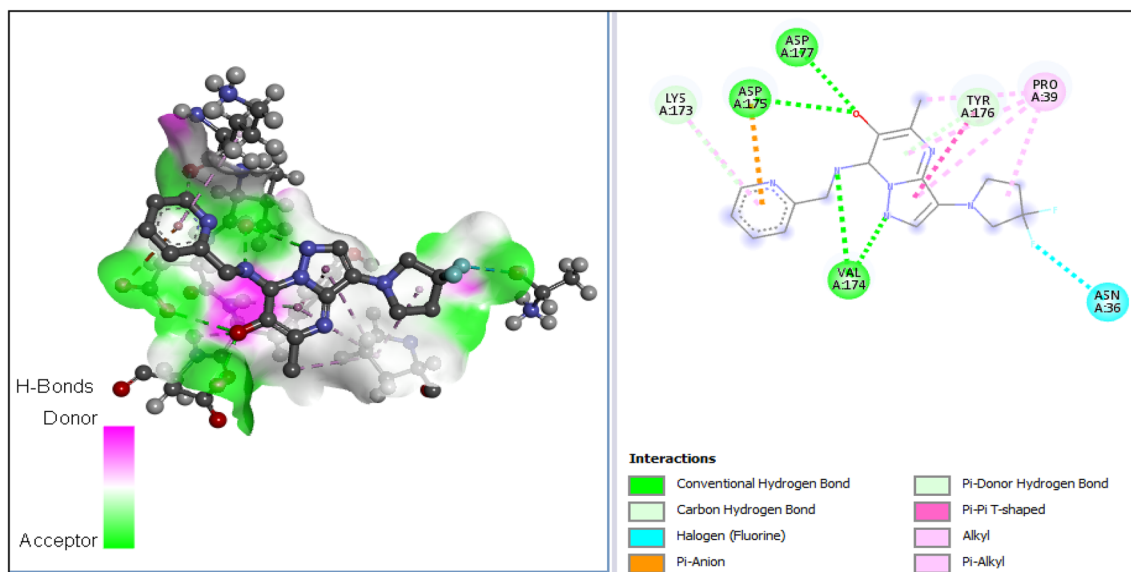
**Table 10** Predicted binding interaction profile of designed compounds with OTU deubiquitinase

Comp. ID	Binding energy (kcal/mol)	Amino acid	Bond type	Interaction	Distance (Å)
<b>A1</b>	− 87.32	ASP-177	Hydrogen bond	Conventional hydrogen bond	2.55
		ASP-177	Hydrogen bond	Conventional hydrogen bond	2.77
		ASP-175	Hydrogen bond	Conventional hydrogen bond	3.30
		VAL-174	Hydrogen bond	Conventional hydrogen bond	2.68
		VAL-174	Hydrogen bond	Conventional hydrogen bond	3.10
		LYS-173	Hydrogen bond	Carbon hydrogen bond	3.30
		TYR-176	Hydrogen bond	$\pi$ -donor hydrogen bond	2.86
		PRO-39	Hydrophobic	alkyl	4.69
		PRO-39	Hydrophobic	Pi-alkyl	4.33
		PRO-39	Hydrophobic	Pi-alkyl	5.11
		PRO-39	Hydrophobic	Pi-alkyl	5.45
		LYS-173	Hydrophobic	Pi-alkyl	4.76
		TYR-176	Hydrophobic	Pi-pi T-shaped	4.40
		TYR-176	Hydrophobic	Pi-pi T-shaped	4.49
		ASP-175	Hydrophobic	Pi-anion	4.27
		ASN-36	Halogen	Fluorine	3.69
<b>A2</b>	− 85.04	ASP-125	Hydrogen bond	Conventional hydrogen bond	2.60
		ASP-127	Hydrogen bond	Conventional hydrogen bond	2.90
		GLU-145	Hydrogen bond	Conventional hydrogen bond	2.75
		LEU-190	Hydrophobic	Alkyl	4.17
		LEU-190	Hydrophobic	Pi-alkyl	5.26
		LEU-160	Hydrophobic	Pi-alkyl	5.44
		ASP-127	Hydrophobic	Pi-anion	3.27
<b>A3</b>	− 86.01	VAL-174	Hydrogen bond	Conventional hydrogen bond	2.82
		VAL-174	Hydrogen bond	Conventional hydrogen bond	3.02
		ASP-177	Hydrogen bond	Carbon hydrogen bond	2.83
		TYR-176	Hydrogen bond	Pi-donor hydrogen bond	3.03
		PRO-37	Halogen	Fluorine	3.30
		HIS-157	Halogen	Fluorine	3.31
		PRO-39	Hydrophobic	Pi-alkyl	4.43
		PRO-39	Hydrophobic	Pi-alkyl	5.24
		ALA-168	Hydrophobic	Pi-alkyl	4.63
		LYS-173	Hydrophobic	Pi-alkyl	4.67
		VAL-174	Hydrophobic	Pi-alkyl	5.12
		TYR-176	Hydrophobic	Alkyl	5.44
		HIS-157	Hydrophobic	Alkyl	4.36
		TYR-176	Hydrophobic	Pi-pi T-shaped	4.46
TYR-176	Hydrophobic	Pi-pi T-shaped	4.50		
<b>A4</b>	− 84.87	LEU-190	Hydrogen bond	Conventional hydrogen bond	2.82
		SER-121	Hydrogen bond	Conventional hydrogen bond	2.93
		TRP-123	Hydrogen bond	Pi-donor	2.86
		TRP-123	Hydrophobic	Pi-pi stacked	4.10
		TRP-123	Hydrophobic	Pi-pi stacked	5.13
		TRP-123	Hydrophobic	Pi-pi stacked	5.40
		TRP-123	Hydrophobic	Pi-alkyl	4.25
		TRP-123	Hydrophobic	Pi-alkyl	4.93
		ASP-116	Halogen	Fluorine	3.46
		LEU-190	Hydrophobic	Alkyl	4.63
		ARG-122	Hydrophobic	Pi-alkyl	4.78

**Table 10** (continued)

Comp. ID	Binding energy (kcal/mol)	Amino acid	Bond type	Interaction	Distance (Å)
<b>A5</b>	− 78.70	GLN-60	Hydrogen bond	Conventional hydrogen bond	2.60
		GLN-60	Hydrogen bond	Conventional hydrogen bond	3.10
		GLU-208	Hydrophobic	Pi-anion	4.44
		ARG-59	Hydrophobic	Pi-cation	4.31
		LEU-196	Hydrophobic	Pi-alkyl	4.87
<b>A6</b>	− 85.73	PHE-192	Hydrogen bond	Conventional hydrogen bond	2.74
		GLY-49	Hydrogen bond	Conventional hydrogen bond	2.95
		HIS-191	Hydrogen bond	Carbon hydrogen bond	2.28
		ILE-48	Halogen	Fluorine	3.61
		PHE-192	Halogen	Fluorine	2.67
		HIS-191	Hydrophobic	Pi-alkyl	5.00
		CYS-53	Hydrophobic	Pi-alkyl	4.42
		GLY-49	Hydrophobic	Amide-pi stacked	4.22
		ASN-50	Hydrophobic	Van der Waals	–
Doxycycline	− 83.70	THR-109	Hydrogen bond	Conventional hydrogen bond	3.23
		SER-121	Hydrogen bond	Conventional hydrogen bond	3.27
		ASP-116	Hydrogen bond	Conventional hydrogen bond	3.38
		ARG-122	Hydrogen bond	Conventional hydrogen bond	2.78
		ARG-122	Hydrogen bond	Conventional hydrogen bond	1.96
		TYR-113	Hydrogen bond	Carbon hydrogen bond	2.83
		ARG-122	Hydrogen bond	Carbon hydrogen bond	2.75
		ARG-122	Hydrogen bond	Carbon hydrogen bond	2.13
		ARG-122	Hydrogen bond	Carbon hydrogen bond	2.98
		ASP-116	Hydrophobic	Pi-anion	3.77

ALA alanine, ARG arginine, ASN asparagine, ASP aspartic acid, GLN glutamine, GLU glutamic acid, GLY glycine, HIS histidine, ILE isoleucine, LEU leucine, LYS lysine, PHE phenylalanine, PRO proline, SER serine, THR threonine, TRP tryptophan, TYR tyrosine, VAL valine

**Fig. 9** 2-D and 3-D view of the interaction between OTU deubiquitinase and **A1**

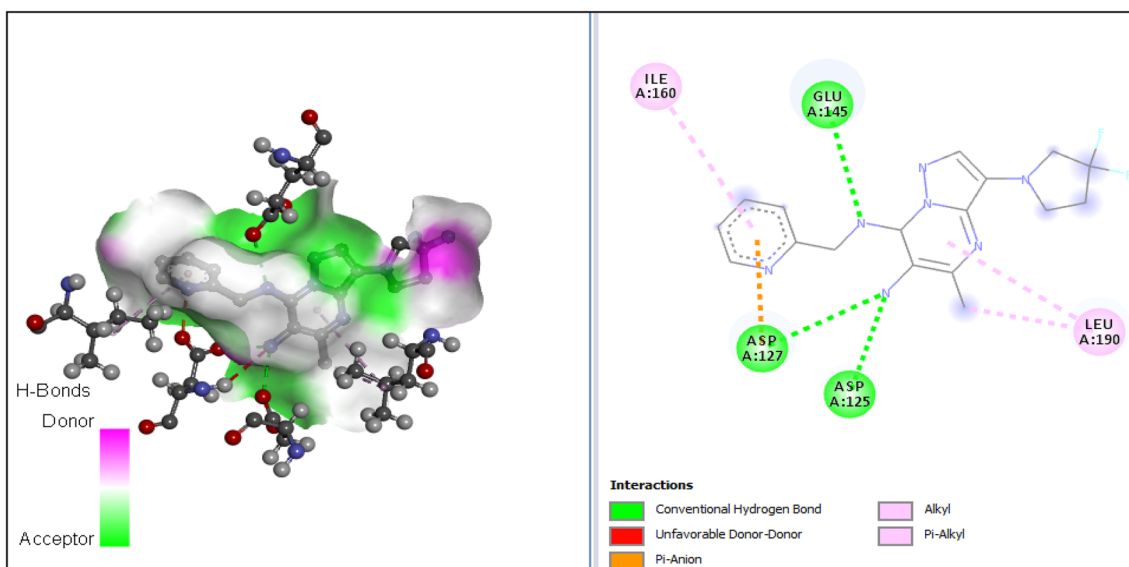


**Fig. 10** 2-D and 3-D view of the interaction between OTU deubiquitinase and **A2**

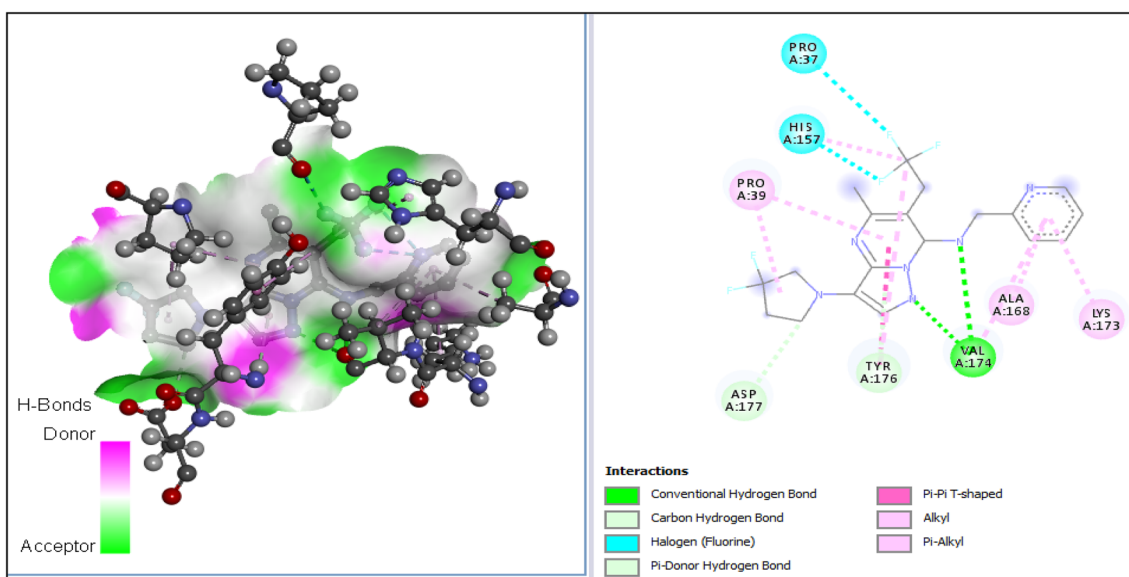


**Fig. 11** 2-D and 3-D view of the interaction between OTU deubiquitinase and **A3**

bio-available, and as well as skin permeable. The molecular docking results showed stronger binding affinities between OTU deubiquitinase receptor and all newly designed molecules than the chosen reference drug (doxycycline) with the exception of **A5**, an indicative of good protein–ligand binding interactions. Hence, these new molecules have demonstrated the potential to arrest *Wolbachia* OTU deubiquitinase, thereby cutting down chances of the bacteria survival,

and which in turn affects the growth and viability of the filarial worms (causative agents for lymphatic filariasis and onchocerciasis). These new compounds could therefore be developed as potential drug candidates for the treatment of lymphatic filariasis and onchocerciasis. More so, laboratory tests (in vitro and in vivo) could be conducted to validate the computational results.

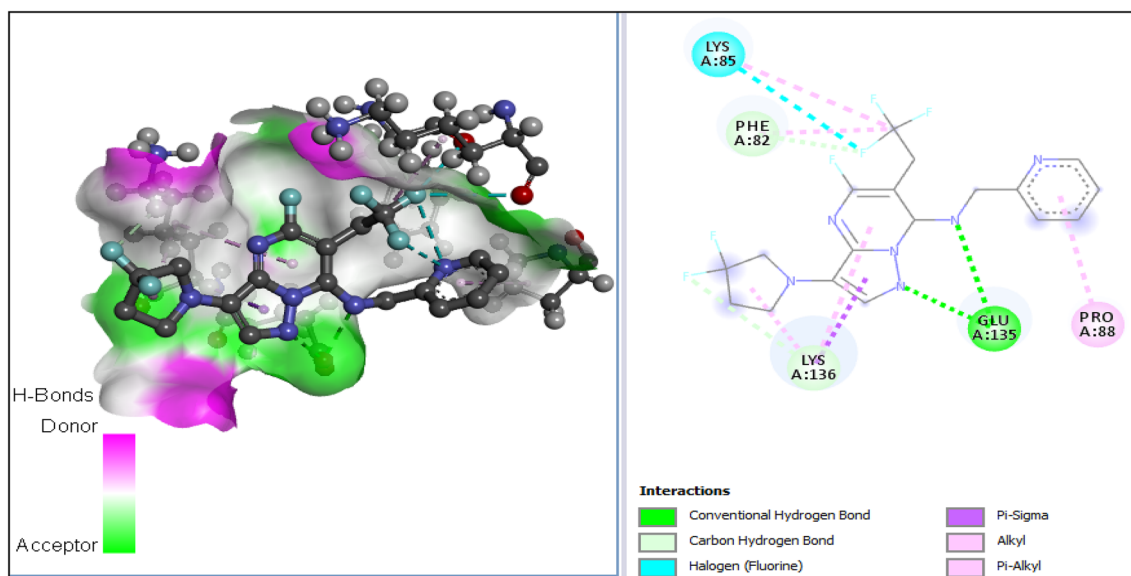


**Fig. 12** 2-D and 3-D view of the interaction between OTU deubiquitinase and A4

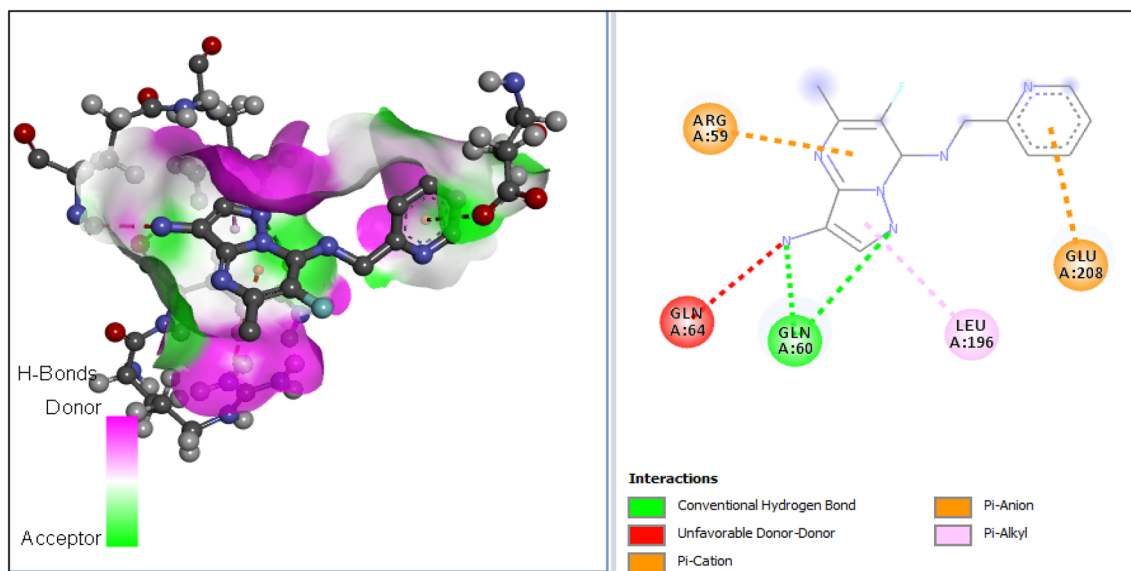


**Fig. 13** 2-D and 3-D view of the interaction between OTU deubiquitinase and A5

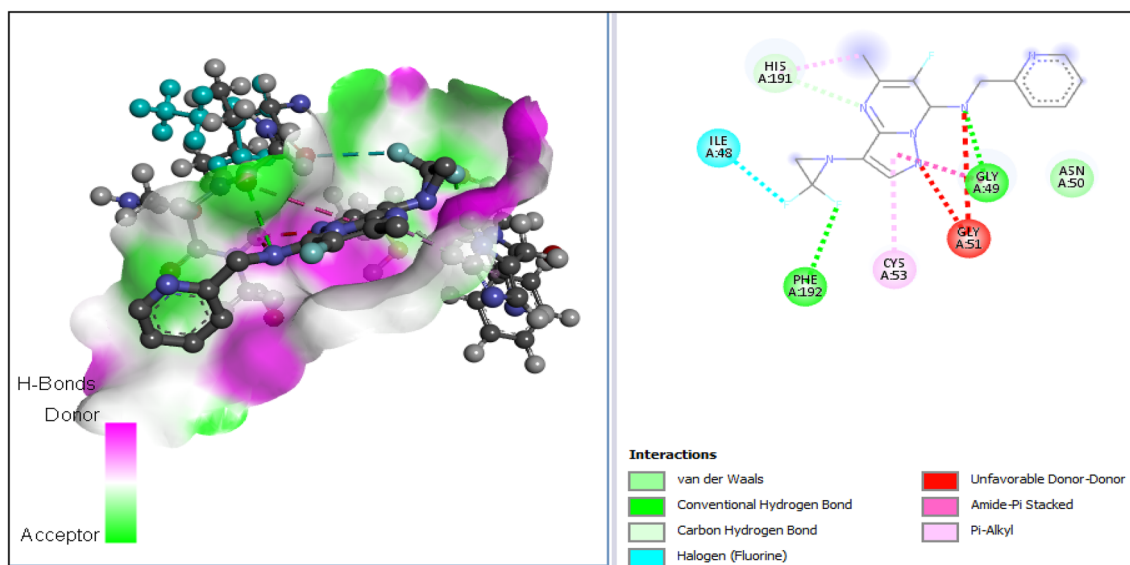


**Fig. 14** 2-D and 3-D view of the interaction between OTU deubiquitinase and A6

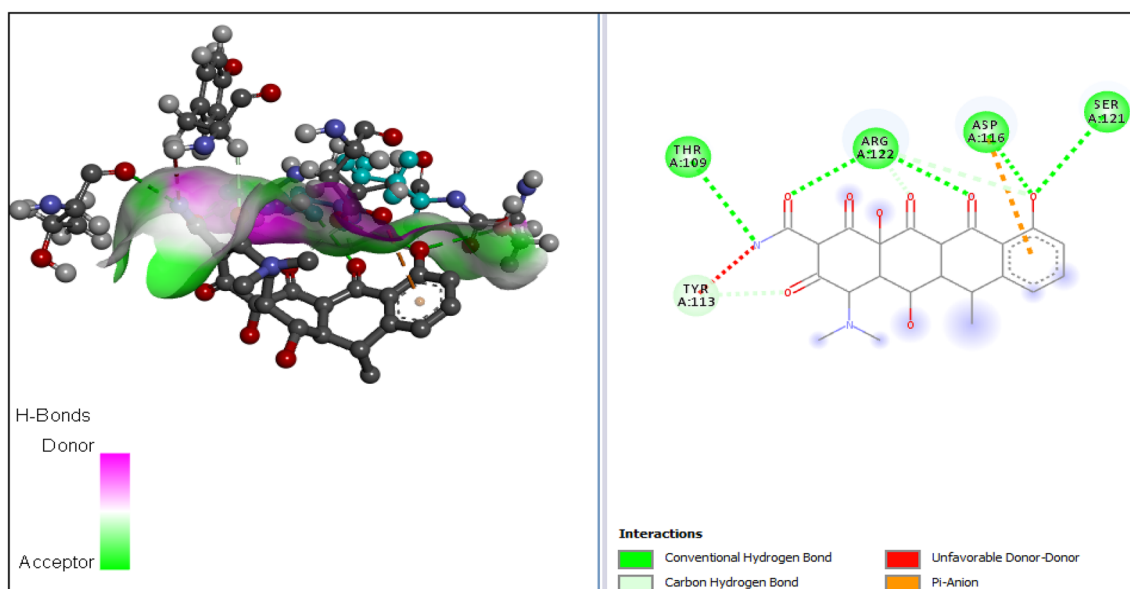


**Fig. 15** 2-D and 3-D view of the interaction between OTU deubiquitinase and Doxycycline

**Acknowledgements** The authors sincerely acknowledge G.F.S. Harrison Quantum Chemistry Research Group, Ahmadu Bello University Zaria, for providing all software used in this study.

**Author contributions** GAS and AU conceived and designed the study. FAU carried out the study and drafted the manuscript. IA conducted the technical editing. All authors read and approved the final manuscript.

**Funding** No funding was received for this study.

**Availability of data and material** All data related to this study are included herein otherwise available on request.

## Declarations

**Conflict of interest** The authors declare that they have no competing interests.

**Ethical approval and consent to participate.** Not applicable.



**Consent for publication** Not applicable.

## References

- Abdullahi A, Shallangwa GA, Ibrahim MT, Bello AU, Arthur DE, Uzairu A, Mamza P (2019) QSAR studies on some C14-urea tetrandrine compounds as potent anti-cancer agents against Leukemia cell line (K562). *JOTCSA* 5(3):1391–1402
- Adawara SN, Shallangwa GA, Mamza PA, Ibrahim A (2020) Molecular docking and QSAR theoretical model for prediction of phthalazinone derivatives as new class of potent dengue virus inhibitors. *Beni-Suef Univ J Basic Appl Sci*. <https://doi.org/10.1186/s43088-020-00073-9>
- Adeniji SE, Uba S, Uzairu A (2018) QSAR modeling and molecular docking analysis of some active compounds against mycobacterium tuberculosis receptor (Mtb CYP121). *J Pathog Hindawi* 2018:24–64
- Adeniji SE, Uba S, Uzairu A (2019) Activity modeling of some potent inhibitors against mycobacterium tuberculosis using genetic function approximation approach. *Adiyaman Univ J Sci* 9(1):77–98
- Adeniji SE, Arthur DE, Abdullahi M, Abdullahi A, Ugbe FA (2020) Computer-aided modeling of triazole analogues, docking studies of the compounds on DNA gyrase enzyme and design of new hypothetical compounds with efficient activities. *J Biomol Struct Dyn*. <https://doi.org/10.1080/07391102.2020.1852963>
- Arthur DE, Uzairu A, Mamza P, Abechi SE, Shallangwa GA (2020) Activity and toxicity modeling of some NCI selected compounds against leukemia P388ADR cell line using genetic algorithm-multiple linear regressions. *J King Saud Univ Sci* 32(1):324–331
- Asati V, Anant A, Patel P, Kaur K, Gupta GD (2021) Pyrazolopyrimidines as anticancer agents: a review on structural and target-based approaches. *Eur J Med Chem*. <https://doi.org/10.1016/j.ejmech.2021.113781>
- Bailey-Elkin BA, van Kasteren PB, Snijder EJ, Kikkert M, Mark BL (2014) Viral OTU deubiquitinases: a structural and functional comparison. *PLoS Pathog* 10(3):e1003894. <https://doi.org/10.1371/journal.ppat.1003894>
- Bakowski MA, Shiroodi RK, Liu R, Olejniczak J, Yang B, Gagaring K, Guo H, White PM, Chappell L, Debec A, Landmann F, Dubben B, Lenz F, Struever D, Ehrens A, Frohberger SJ, Sjoberg H, Pionnier N, Murphy E, Archer J, Steven A, Chunda VC, Fombad FF, Chounna PW, Njouendou AJ, Metuge HM, Ndzeshang BL, Gandjui NV, Akumtuh DN, Kwenti TDB, Woods AK, Joseph SB, Hull MV, Xiong W, Kuhen KL, Taylor MJ, Wanji S, Turner JD, Hübner MP, Hoerauf A, Chatterjee AK, Roland J, Tremblay MS, Schultz PG, Sullivan W, Chu XJ, Petrassi HM, McNamara CW (2019) Discovery of short-course anti-wolbachial quinazolines for elimination of filarial worm infections. *Sci Transl Med* 11(491):87. <https://doi.org/10.1126/scitranslmed.aav3523>
- Bouchery T, Lefoulon E, Karadjian G, Nieguitsila A, Martin C (2013) The symbiotic role of wolbachia in onchocercidae and its impact on filariasis. *Clin Microbiol Infect* 19(2):131–140
- Carter DS, Jacobs RT, Freund Y, Berry P, Akama T, Easom EE, Lunde CS, Rock FL, Stefanakis R, McKerrow JH, Fischer C, Bulman C, Lim KC, Suzuki BM, Tricoche N, Sakanari J, Lustigman S, Plattner JJ (2020) Macrolidicidal benzimidazole-benzoxaborole hybrids as an approach to the treatment of river blindness, part 2: ketone linked analogs. *ACS Infect Dis* 6(2):180–185
- Cooper PJ, Nutman TB (2013) Onchocerciasis. In: Magill AJ, Hill DR, Solomon T, Ryan ET (eds) *Hunter's tropical medicine and emerging infectious disease*, 9th edn. WB Saunders, London, pp 827–834
- Edache EI, Samuel H, Sulyman YI, Arinze O, Ayine OI (2020) QSAR and molecular docking analysis of substituted tetraketone and benzyl-benzoate analogs as anti-tyrosine: A novel approach to anti-tyrosine kinase drug design and discovery. *Chem Res J* 5(6):79–100
- Henkle-Duhrsen K, Eckelt VH, Wildenburg G, Blaxter M, Walter RD (1998) Gene structure, activity and localization of a catalase from intracellular bacteria in onchocerca volvulus. *Mol Biochem Parasitol* 96(1–2):69–81
- Hotez PJ, Aksoy S, Brindley PJ, Kamhawi S (2020) What constitutes a neglected tropical disease? *PLoS Negl Trop Dis* 14(1):e0008001
- Ibrahim MT, Uzairu A, Shallangwa GA, Uba S (2020) Lead identification of some anti-cancer agents with prominent activity against Non-small Cell Lung Cancer (NSCLC) and structure-based design. *Chem Afr* 3:1023–1044
- Ibrahim MT, Uzairu A, Uba S, Shallangwa GA (2021) Design of more potent quinazoline derivatives as EGFRWT inhibitors for the treatment of NSCLC: a computational approach. *J Pharm Sci* 7:140
- Imberty A, Hardman KD, Carver JP, Perez S (1991) Molecular modeling of protein-carbohydrate interactions: docking of monosaccharides in the binding site of concanavalin A. *Glycobiology* 1(6):631–642
- Isyaku Y, Uzairu A, Uba S, Ibrahim MT, Umar AB (2020) QSAR, molecular docking, and design of novel 4-(N, N-diarylmethyl amines) Furan-2(5H)-one derivatives as insecticides against *Aphis craccivora*. *Bull Natl Res Centre* 44:44
- Jacobs RT, Lunde CS, Freund YR, Hernandez V, Li X, Xia Y, Carter DS, Berry PW, Halladay J, Rock F, Stefanakis R, Easom E, Plattner JJ, Ford L, Johnston KL, Cook DAN, Clare R, Cassidy A, Myhill L, Tyrer H, Gamble J, Guimaraes AF, Steven A, Lenz F, Ehrens A, Frohberger SJ, Koschel M, Hoerauf A, Hubner MP, McNamara CW, Bakowski MA, Turner JD, Taylor MJ, Ward SA (2019) Boron-Pleuromutilins as anti-wolbachia agents with potential for treatment of onchocerciasis and lymphatic filariasis. *J Med Chem* 62:2521–2540
- Kennard RW, Stone LA (1969) Computer aided design of experiments. *Technometrics* 11:137–148
- Kumar NA, Sharmila R, Akila K, Jaikumar B (2016) In-silico approach for the assessment of oral cancer property on *Limonia acidissima*. *IJPSR* 7(3):1271–1275
- Kurz M, Iturbe-Ormaetxe I, Jarrott R, Cowieson N, Robin G, Jones A, King GJ, Frei P, Glockshuber R, O'Neill SL, Heras B, Martin JL (2008) Cloning, expression, purification and characterization of a DsbA-like protein from wolbachia pipientis. *Protein Expr Purif* 59(2):266–273
- Lakshmi V, Joseph SK, Srivastava S, Verma SK, Sahoo MK, Dube V, Mishra SK, Murthy PK (2010) Antifilarial activity in vitro and in vivo of some flavonoids tested against *Brugia malayi*. *Acta Trop* 116:127–133
- Lawal HA, Uzairu A, Uba S, (2021) QSAR, molecular docking studies, ligand-based design and pharmacokinetic analysis on Maternal Embryonic Leucine Zipper Kinase (MELK) inhibitors as potential anti-triple-negative breast cancer (MDA-MB-231 cell line) drug compounds. *Bull Natl Res Centre* 45(90)
- Li Z, Wan H, Shi Y, Ouyang P (2004) Personal experience with four kinds of chemical structure drawing software: review on ChemDraw, ChemWindow, ISIS/Draw, and ChemSketch. *J Chem Inf Comput Sci* 44:1886–1890
- Lipinski CA, Lombardo F, Dominy BW, Feeney PJ (2001) Experimental and computational approaches to estimate solubility and permeability in drug discovery and development settings. *Adv Drug Deliv Rev* 46:3–26



- McGillan P (2017) Development of small-molecule anti-*wolbachia* agents for the treatment of filariasis. PhD Thesis University of Liverpool. Retrieved from <https://livrepository.liverpool.ac.uk/3016953>
- McGillan P, Berry NG, Nixon L, Leung SC, Webborn PJH, Wenlock MC, Kavanagh S, Cassidy A, Clare RH, Cook DA, Johnston KL, Ford L, Ward SA, Taylor MJ, Hong WD, O'Neill PM (2021) Development of pyrazolopyrimidine anti-*wolbachia* agents for the treatment of filariasis. *ACS Med Chem Lett* 12(9):1421–1426
- Roy K, Chakraborty P, Mitra I, Ojha PK, Kar S, Das RN (2013) Some case studies on application of “rm2” metrics for judging quality of quantitative structure–activity relationship predictions: emphasis on scaling of response data. *J Comput Chem* 34(12):1071–1082
- Schubert AF, Nguyen JV, Franklin TG, Geurink PP, Roberts CG, Sanderson DJ, Miller LN, Ovaas H, Hofmann K, Pruneda JN, Komander D (2020) Identification and characterization of diverse OUT deubiquitinases in bacteria. *EMBO J* 39:e105127
- Sliwoski G, Kothiwale S, Meiler J, Lowe EW (2014) Computational methods in drug discovery. *Pharmacol Rev* 66:334–395
- Sun Y, Yang AW, Hung A, Lenon GB (2020) Screening for a potential therapeutic agent from the herbal formula in the 4th edition of the Chinese national guidelines for the initial-stage management of COVID-19 via molecular docking. *Evid Based Complement Alternat Med* 2020:3219840
- Townson S, Hutton D, Siemienska J, Hollick L, Scanlon T, Tagboto SK, Taylor MJ (2000) Antibiotics and *wolbachia* in filarial nematodes: antifilarial activity of rifampicin, oxytetracycline and chloramphenicol against *onchocerca gutturosa*, *onchocerca lienalis* and *brugia pahangi*. *Ann Trop Med Parasitol* 94(8):801–816
- Tropsha A, Gramatica P, Gombar VK (2003) The importance of being earnest: validation is the absolute essential for successful application and interpretation of QSPR models. *Mol Inform* 22:69–77
- Ugbe FA, Shallangwa GA, Uzairu A, Abdulkadir I (2021) Activity modeling, molecular docking and pharmacokinetic studies of some boron-pleuromutilins as anti-*wolbachia* agents with potential for treatment of filarial diseases. *Chem Data Collect* 36:100783
- Veerasingam R, Rajak H, Jain A, Sivadasan S, Varghese CP, Agrawal RK (2011) Validation of QSAR models-strategies and importance. *Int J Drug Des Discov* 3:511–519
- Wang X, Dong H, Qin Q (2020) QSAR models on aminopyrazole-substituted resorcylic compounds as Hsp90 inhibitors. *J Comput Sci Eng* 48:1146–1156
- Wilsher EJ (2011) The impact of neglected tropical diseases, and their associated stigma, on people's basic capabilities. Durham E-Theses Online. <http://etheses.dur.ac.uk/3301/>

**Publisher's Note** Springer Nature remains neutral with regard to jurisdictional claims in published maps and institutional affiliations.